Pergamon

J. Biomechanics, Vol. 28, No. 10, pp. 1179–1191, 1995

0021–9290/95 $9.50 + .00

0021-9290(94)00181-2

THE CONTROL OF SHOULDER MUSCLES DURING GOAL DIRECTED MOVEMENTS, AN INVERSE DYNAMIC ANALYSIS

R. Happee* and F. C. T. Van der Helm

Man-Machine-Systems Group, Delft University of Technology, Faculty of Mechanical Engineering & Marine Technology, Mekelweg 2, 2628-CD Delft, The Netherlands

Abstract—Fast goal directed arm movements in the sagittal plane were analyzed with a three-dimensional shoulder model with 95 muscle elements. Dynamics of the muscle elements were described by a third-order nonlinear muscle model. Muscle forces and activation were estimated using the method of inverse muscular dynamics, an optimization scheme which uses only very limited computational power.

Most model results were similar to the EMG but some differences between model results and EMG were found in muscles where the EMG activity was subject dependent.

For the movement studied, the thoracoscapular muscles were shown to deliver about 40% of the energy required for the acceleration of the arm during anteflexion and about 22% during retroflexion. Activity of thoracoscapular muscles was also required to ensure contact between the thorax and the scapula which is important for the mechanical stability of the shoulder. The rotator cuff muscles were found to deliver about 19% of the energy required for the acceleration of the arm during anteflexion and about 8% during retroflexion.

INTRODUCTION

The shoulder is a complex mechanical structure containing several joints connecting the humerus, the scapula, the clavicle and finally the sternum (Fig. 1). Furthermore, the scapula contacts the dorsal part of the thorax; it can glide over the so-called scapulothoracic gliding plane. This connection makes the shoulder a closed chain mechanism. As a result, the clavicle and thorax constrain the scapular rotations, and in addition, the moments about the sternoclavicular and acromioclavicular joint are coupled. The complexity of the shoulder makes it very difficult to understand muscular coordination of the shoulder, or even to comprehend the motions of shoulder bones.

Until now, the shoulder has been studied mainly in static conditions. Three-dimensional positions of the arm and the bones of the shoulder girdle have been recorded for a number of abduction and anteflexion angles of the humerus (Pronk, 1991; Pronk and Van der Helm, 1991; Van der Helm and Pronk, 1994). The relation between the rotations of humerus and scapula is commonly referred to as the 'scapulohumeral rhythm' (Högfors *et al.*, 1991; Inman *et al.*, 1944: Pronk, 1989, 1991). This relation is reasonably consistent and reproducible, although the assessed values of the rotations of the scapula and the humerus show some individual variations, and show a dependency on the measurement equipment (roentgen versus goniometers) and the experimental paradigm (two-dimensional versus three-dimensional). EMG studies in static conditions have provided information about the coordinated activity of shoulder muscles (Flanders and Soechting, 1990; Inman *et al.*, 1944). The mechanical function of such muscular activity has been analyzed with three-dimensional models (Karlsson and Peterson, 1992; Van der Helm, 1994a, b).

The coordination of shoulder muscles in dynamic conditions has been studied experimentally in Happee (1992b). Goal directed arm movements in the sagittal plane, mainly consisting of an anteflexion or retroflexion in the shoulder (more formally described as anteflexion/retroflexion of the glenohumeral joint) have been studied. The EMG of 13 muscles in the shoulder and the arm has been recorded. Triphasic activation patterns associated with acceleration and deceleration of the limb have been found in muscles which can be regarded as prime movers of the glenohumeral joint (deltoideus, pectoralis and latissimus dorsi). The patterns in thoracoscapular muscles were very similar to patterns in these prime movers of the glenohumeral joint. This indicates a function of thoracoscapular muscles in the acceleration of the arm which is also supported by a statistical analysis of EMG and kinematics (Happee, 1993a). Antagonist activity was rare in the EMG of thoracoscapular muscles. Thus it is not clear in which way decelerating forces induced by the prime movers are transferred to the trunk (Happee, 1992b).

Such EMG studies have considerable limitations. Recording the EMG of deeper lying muscles yields severe technical problems, especially in dynamic conditions and for smaller muscles. EMG provides no information on the forces occurring in joints and

Received in final form 14 *November* 1994.

*Current address: TNO Crash-Safety Research Centre, Biomechanics Section, Schoemakerstraat 97, 2628-VK Delft, The Netherlands.

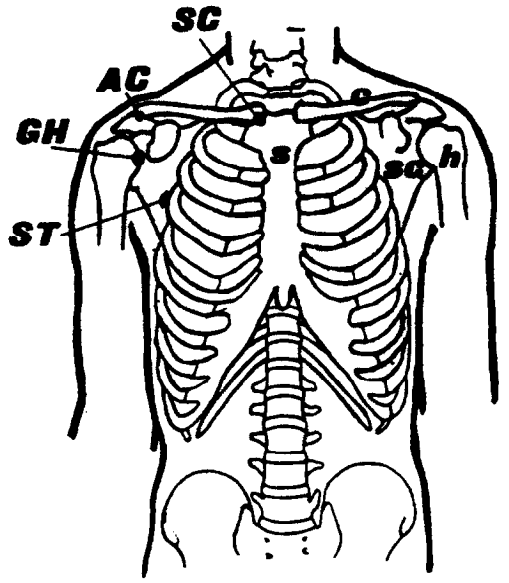

Fig. 1. Frontal view of the upper part of the body. The bones indicated are: the humerus (h), the clavicle (c), the scapula (sc) and the sternum (s), The articulations indicated are: the sternoclavicular joint (SC), the acromioclavicular joint (AC), the glenohumeral joint (GH) and the scapulothoracic gliding plane (ST); reprinted with permission from Pronk (1989).

ligaments. EMG can show when muscles are active but cannot explain the mechanical function of this activity.

For these reasons it was decided to analyze the goal directed movements studied in Happee (1992b) using a detailed musculoskeletal model. The goal of this simulation study was to provide insight into the function of shoulder muscles. The first question studied is in how far the different muscles contribute mechanical energy for the acceleration/deceleration of the arm. Here the thoracoscapular muscles, which only indirectly affect the arm, are of particular interest. The second question studied is how the scapula and the glenohumeral joint are being stabilized.

METHODS

A three-dimensional model of bones and ligaments

To analyze displacements of the shoulder, a kinmatic model of the shoulder girdle was developed by Pronk (1989, 1991). To permit analysis of muscle forces, the model was transformed into a dynamic model (Veeger *et al.*, 1991; Van der Helm and Veenbaas, 1991; Van der Helm *et al.*, 1992; Van der Helm, 1994a, b). In the model the thorax, clavicle, scapula, humerus and forearm are represented as rigid bodies. Motion constraints of the scapulothoracic gliding plane are included. This model contains 20 muscles, divided into a total 95 muscle elements as shown in Table 1. Muscle lines of action curve around underlying bony contours. In addition to this existing model, for the current paper, the effects of nonlinear muscular dynamics are included by using the method of inverse muscular dynamics (Happee, 1994). The resulting shoulder model will now be described in more detail.

Degrees of freedom (DOF): The sternoclavicular, acromioclavicular and glenohumeral joints are described as spherical joints each having three DOF. The elbow is described as a joint with only one DOF which is elbow flexion. The conoid ligament constrains the motions of the clavicle with respect to the scapula. As the conoid ligament is assumed stiff this yields one kinematic constraint. The scapulothoracic

Table 1. Number of elements, physiological cross-sectional area (PCSA) per element and location order of the elements for future reference in figures, for the muscles of the shoulder mechanism

Muscle (part)	No. of elements	PCSA/element (cm^2)	Element order
Trapezius pars scapularis	6	2.39	Caudal–cranial
Trapezius pars clavicularis	6	0.52	Caudal–cranial
Levator scapulae	3	1.15	Caudal–cranial
Pectoralis minor	4	0.86	Medial–lateral
Rhomboideus	3	2.52	Caudal–cranial
Serratus anterior	6	1.90	Caudal–cranial
Deltoideus pars scapularis	6	2.76	Medial–lateral
Deltoideus pars clavicularis	6	1.35	Lateral–medial
Coracobrachialis	6	0.53	Lateral–medial
Infraspinatus	6	1.36	Cranial–caudal
Teres minor	6	0.52	Cranial–caudal
Teres major	6	2.09	Cranial–caudal
Supraspinatus	6	0.78	Ventral–dorsal
Subscapularis	6	2.50	Cranial–caudal
Biceps brachii caput longum	1	3.12	
Biceps brachii caput breve	1	3.12	
Triceps brachii caput longum	2	3.12	Medial–lateral
Latissimus dorsi	5	1.70	Cranial–caudal
Pectoralis major pars thoracalis	5	1.74	Caudal–cranial
Pectoralis major pars clavicularis	5	0.71	Medial–lateral

gliding plane is modeled by two surface elements at the angulus inferior (AI) and the trigonum spinae (TS) of the scapula, respectively, It is assumed that during the active arm movements studied, contact at these two surface elements is maintained. This contact yields two kinematic constraints. How this contact will be maintained will be treated in the following section. The sternoclavicular, acromioclavicular, glenohumeral and elbow joints yield 10 DOF, the conoid ligament and the scapulothoracic gliding plane impose 3 kinematic constraints which yields a model with 7 kinematic DOF. This specifies 7 equality constraints relating muscle forces to joint torques. Furthermore, the model contains 4 inequality constraint on the muscular forces which will now be treated.

Linear inequality constraints: The conoid ligament can practically transfer only tension forces, which is taken into account by one inequality constraint (Van der Helm, 1994a). The forces at the scapulothoracic gliding plane have to be compression forces which yields two inequality constraints for AI and TS, respectively.

Glenohumeral constraint: The glenohumeral joint has been implemented as a spherical joint with three rotational DOF, not allowing translation (e.g. dislocation). A constraint on muscle forces, preventing dislocation will now be described. The passive structures in and around the glenohumeral joint do not guarantee joint stability (Lippitt and Matsen, 1993). It is assumed that the glenohumeral joint is actively stabilized; the surrounding muscles have to be controlled so as to prevent dislocation. Stability of the glenohumeral joint has been included as a nonlinear constraint as described in Van der Helm (1994a). Stability is obtained if the reaction forces point inside the glenoid. The rim of the glenoid joint surface has been described as an ellipse. Muscular forces have been constrained so that the net joint reaction force is directed from the joint rotation center to any point within this ellipse. If the reaction force vector would point outside the glenoid, it could not be counteracted by the glenoid reaction force and dislocation would result.

Elbow function: The model includes the bi-articular biceps brachii caput longum and triceps brachii caput longum and caput breve. This provides only a limited set of elbow muscles. For the movement studied here, for acceleration and deceleration of the limb, large torques are required in the shoulder whereas in the elbow a small nearly constant torque is required (Happee, 1992b). For these reasons the movement equation prescribing the elbow torque has been disregarded. The kinematic degree of freedom is left in the model. Thus 6 out of the 7 linear equality constraints representing the movement equations will be considered. Three linear inequality constraints represent both capulothoracic forces and the conoid ligament force. The stability of the glenohumeral joint yields one nonlinear inequality constraint. Muscle forces will be chosen such that these constraints are being met. This will ensure that the assumptions made defining the DOF are valid. Muscle forces will always be positive or zero, yet muscular dynamics impose further constraints on muscle forces as will be described in a following section.

Muscle model

A nonlinear, lumped-parameter model of muscular dynamics is employed which has been presented in Happee (1994) and which is largely based on Winters and Stark (1985, 1988). The model contains a first-order description of neural-excitation dynamics and a first-order active-state dynamics. The third order emerges from the force–velocity relation (Hill curve) combined with a series elastic element (SE). An active force–length relation is not yet implemented as major problems occurred in the choice of muscle lengths at which maximal active force is delivered. This is acceptable as for the current paper only relatively small changes of muscle length are considered. For similar reasons the model does not contain a passive force–length relation describing a parallel elastic element (PE) which is justified because for this paper no extreme joint angles are considered (Engin, 1980). Information on muscle properties like the slow/fast fiber composition was not available for all muscles considered, therefore muscle parameters were chosen according to an average fiber composition (Winters and Stark, 1985). The minimal active state A_{min} was taken as the resting active state from Hatze (1981). The parameters are given in Table 2, where the muscular physiological cross-sectional area (PCSA) was

Table 2. Normalized muscular parameters as a function of muscle size, PCSA = physiological cross-sectional area in cm^2, L_{t0} = total rest length, L_0 = muscle fiber rest length

Description	Parameter		Value
Maximal isometric force	F_{max}	[N]	100 PCSA
Minimal or resting active state	A_{min}	[ ]	0.005
Series elastic stretch with maximal isometric force	SE_{xm}	[m]	0.05 L_{t0}
Series elastic shape parameter	SE_{sh}	[ ]	3
Hill, maximal shortening velocity	MV_{vm}	[$m s^{-1}$]	5 L_0
Hill, shape parameter	MV_{sh}	[ ]	0.25
Time constant increasing active state	T_{ac}	[ms]	10
Time constant decreasing active state	T_{da}	[ms]	50
Time constant neural excitation	T_{ne}	[ms]	40

chosen according to Table 1 and the rest length (L_{t0}) was taken from Van der Helm *et al.* (1992). In accordance with dissection studies the mean fiber rest length L_0 was taken as 33% of L_{t0} for the distal muscles (biceps brachii and triceps brachii) and 75% for the other muscles (Karlsson, 1992).

Dynamic constraint derived with inverse muscular dynamics

A new method for estimating muscular force and activation from experimental kinematic data was presented in Happee (1994). The method combines conventional inverse dynamics with optimization utilizing a dynamic muscle model. The method uses only very limited computational power, which makes it a useful tool especially for more complex systems. The net torques/forces are calculated by using conventional inverse dynamics. Then, a solution of the load sharing problem is determined by optimization (minimization or maximization) of a cost criterion. This yields an inverse dynamic optimization. The solution determined is such that it satisfies a dynamic physiological constraint on muscular force. This dynamic constraint is determined with the inverse of the nonlinear muscle model described in the previous section and thus takes into account the muscle properties described in this section. With this model muscular states and neural inputs are also estimated.

The criterion for the load sharing problem

The load sharing problem is solved by minimization of a metabolic cost criterion. Such a criterion can represent the metabolic cost of muscle contraction but can also be task dependent. Several criteria have been proposed in the literature (Pedotti, 1978; Crowninshield and Brand, 1981; Patriarco *et al.*, 1981; Dul *et al.*, 1984a, b; Pedersen *et al.*, 1987). In Happee and van der Helm (1994) experimental support is provided for a quadratic criterion, physiological support is provided for a weighting of muscle volume (V) and it is shown that such a weighting contributes to similar stresses in synergist muscles. This yields the following criterion:

$$J = \sum_{j=1}^{N} V_j \left(\frac{F_j}{F_{\max j}} \right)^2. \quad (1)$$

Here j is the muscle number and F/F_{max} represents the active state which is related to the calcium ion concentration and hence to the muscular energy consumption. In dynamic conditions, F_{max} will be time dependent due to the physiological force–velocity relation and, when implemented, the force–length relation.

Kinematic and EMG data

Maximally fast goal directed movements were performed with a set-up described in Ruitenbeek and Jansen (1984) and Happee (1992b). With their right arm the subjects controlled a manipulator with one degree of freedom; a forward or backward movement of the hand. The arm was held in the sagittal plane, the forearm stayed roughly horizontal and the upper arm ranged between about 20° anteflexion and 15° retroflexion. As the model includes muscular dynamics it is suitable for analysis of such fast movements. Such experiments were performed with 18 healthy male subjects from the student population (Happee, 1992b, 1993b and unpublished results). A very tight relation exists between the kinematic and the EMG timing. As this relation would be obscured by averaging, individual movements were analyzed with the shoulder model. One maximally fast anteflexion (forward) and one retroflexion (backward) movement were analyzed. The subject was from Happee (1993b) and was selected because he moved relatively fast as compared to other subjects (but not extremely fast). The movements were selected as to have no abnormalities in the kinematic signals. This means that they had a small overshoot and no subsequent fluctuations. The muscle activity predicted with the model will be compared with surface EMG recorded during these movements. Some EMG results from the other subjects will be also discussed. The muscles studied are: deltoideus pars anterior, media and posterior, latissimus dorsi, pectoralis major pars clavicularis and thoracalis, serratus anterior, trapezius pars transversalis, infraspinatus and biceps brachii.

Bi-polar surface EMG was recorded with disposable Ag/AgCl electrodes with an inter-electrode distance of 23 mm directly attached to a pre-amplifier. The signal was bandpass filtered from 20–1500 Hz, rectified and low-pass filtered (100 Hz). These EMG signals were sampled at 250 Hz, together with the position and velocity of the hand and the force exerted by the hand.

As input variables the method of inverse dynamics requires the position, velocity and acceleration signals for every degree of freedom. The position of the hand was recorded. This noisy signal was processed as described in Happee (1994), yielding kinematic data with a time-step of 12 ms shown in Fig. 2. This processing is essential because the method of inverse

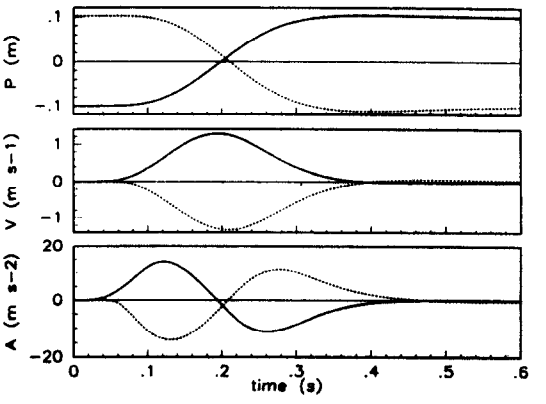

Fig. 2. Kinematic data of the anteflexion (——) and the retroflexion (· · ·) movement, P = hand position, V = velocity, A = acceleration.

dynamics involves multiple differentiations which would give unacceptable effects of measurement noise.

The set-up does not constrain adduction/abduction. If necessary the experimenter instructed subjects to keep the arm in the sagittal plane. Therefore the position of the elbow was computed assuming that the arm was held in the sagittal plane. The movements of the scapula and the clavicle could not be measured in these fast movements. Therefore shoulder bone positions were chosen according to static measurements. These measurements were performed with the palpator, an instrument for measuring 3-D positions of bony landmarks (Pronk and Van der Helm, 1991). Shoulder bone positions at zero degrees anteflexion were chosen according to Van der Helm and Pronk (1994). As discussed in the introduction, in static experiments a reasonably consistent relation has been found between the rotations of humerus and scapula. This relation is commonly referred to as the 'scapulohumeral rhythm'. Based on the results of Inman *et al.* (1944) and Pronk (1991) we assumed the medial/lateral-rotation of the scapula to be one-third of the rotation of the humerus. As described in the section *Degrees of freedom* the assumed motions of the scapula are such that contact with the thorax is maintained at the angulus inferior (AI) and the trigonum spinae (TS). This derivation of scapular movement is described in detail in Van der Helm (1994b).

RESULTS

Muscular dynamics

Figure 3 shows the effect of the dynamic constraint imposed by muscular dynamics on the neural inputs and stresses predicted. Both the inverse dynamic solution including muscular dynamics and the conventional inverse dynamic solution which ignores muscular dynamics are given. An agonist force is required between about $t = 0.05$ s and $t = 0.20$ s as can be seen from the unconstrained simulation (Fig. 3, right upper plot, dotted trace). However, muscular dynamics constrain the rate of force decrease (Fig. 3, right upper plot, continuous trace. The slowly decaying agonist forces have to be compensated for by increased antagonist forces (Fig. 3, lower right plot, continuous trace). The predicted neural muscular inputs in the left plots of Fig. 3 show the well-known triphasic pattern. A comparison of the inputs predicted with and without the dynamic constraint, once more shows the relevance of muscular dynamics.

Comparison of model predictions with EMG

Figure 4 shows neural inputs estimated with the model and the rectified surface EMG of the corresponding muscle parts. With the model, neural inputs were estimated from the kinematic data of the movements from which these EMG signals were recorded. The model inputs and EMG signals in Fig. 4 will be compared, also taking into account the EMG recorded in identical experiments in 18 other subjects (Happee, 1992b, 1993b; and unpublished results).

Deltoideus: In Fig. 4a both the simulated and the EMG activity of the deltoideus pars anterior, media and posterior show the well-known difference in function between these muscle parts (e.g. Bassett *et al.*, 1990; Flanders and Soechting, 1990). In the simulations the other elements of the deltoideus showed an intermediate activity. The agonist EMG activity in the deltoideus pars anterior during anteflexion and in the deltoideus pars posterior during retroflexion corresponds well with the predicted model inputs. In the EMG of these muscles, antagonist activity is not very clear in Fig. 4a. However, in other subjects such antagonist activity was more pronounced. In the deltoideus pars media no clear activity was found in both the model predictions and the EMG.

Latissimus dorsi: Figure 4b shows differences between the predicted activity for three elements of the latissimus dorsi. The other elements showed an intermediate behavior. The EMG was recorded in a position matching the middle element (lati3). Figure 4b

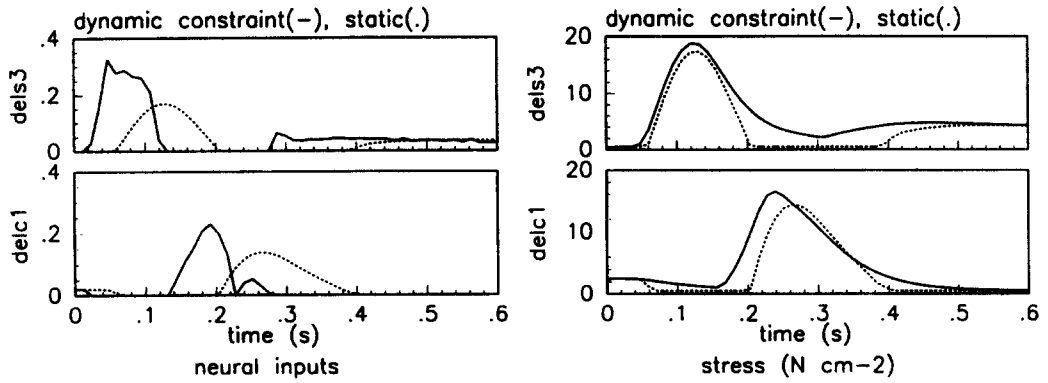

Fig. 3. The effect of the dynamic constraint imposed by muscular dynamics for two parts of the deltoideus showing agonist (upper traces) and antagonist activity (lower traces) during retroflexion, left column = neural inputs, right column = stress, (——) simulated with muscular dynamics, (· · ·) simulated without muscular dynamics where the neural input simply describes the force relative to the maximal force.

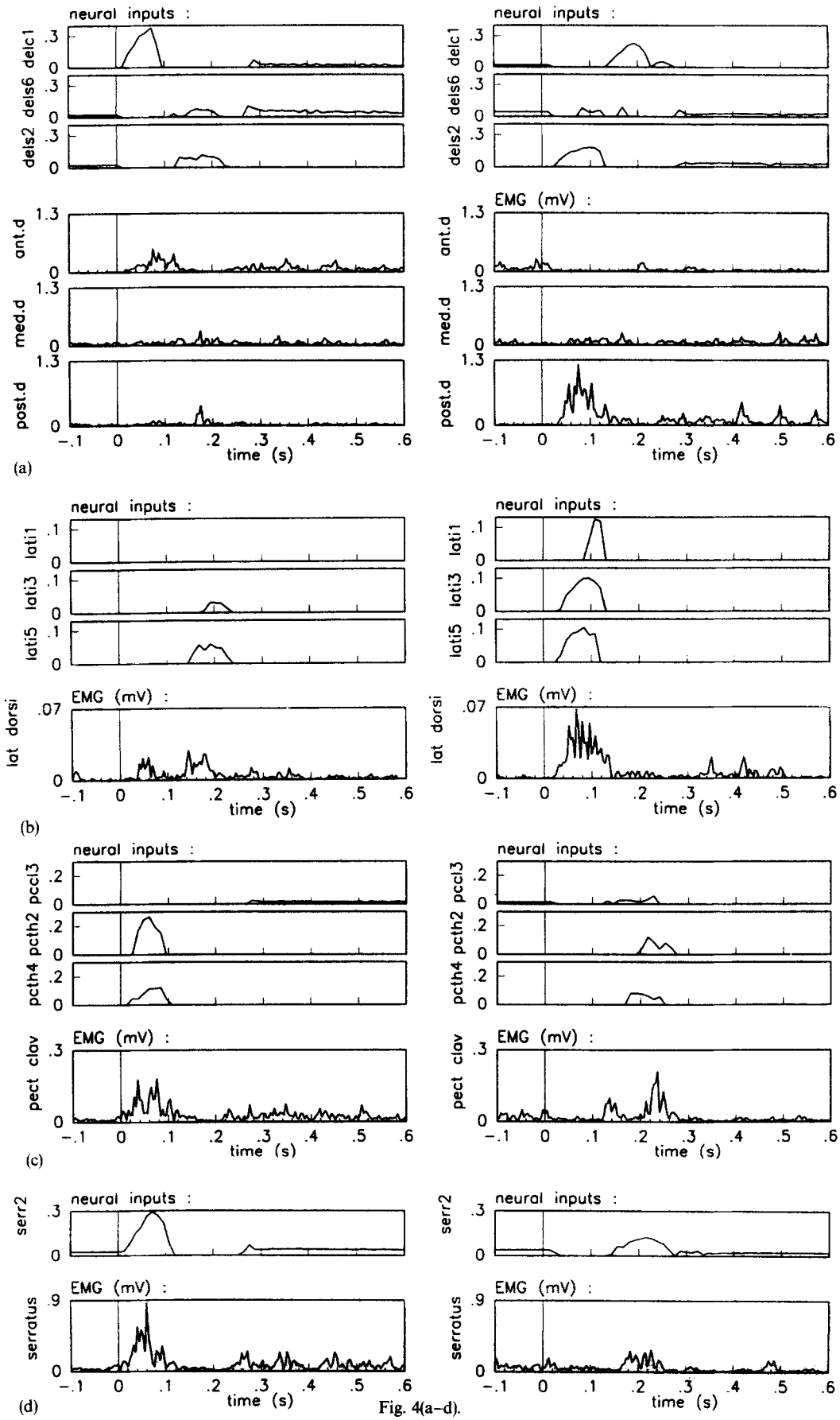
neural inputs :
delc1
dels6
dels2
EMG (mV) :
ant.d
med.d
post.d
time (s)
(a)
lati1
lati3
lati5
lat dorsi
(b)
pcch3
pcth2
pcth4
pect clav
(c)
serr2
serratus
(d)

Fig. 4(a–d).

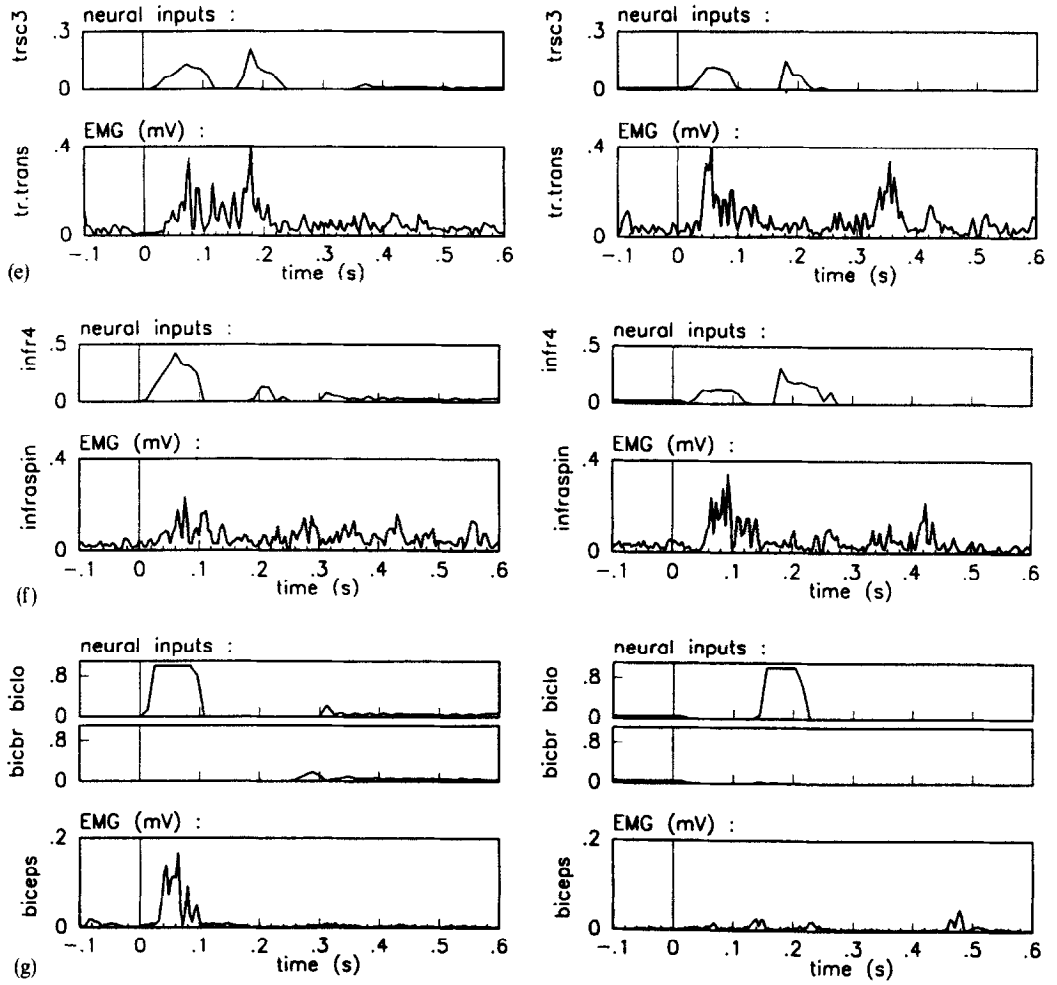

Fig. 4. Validation: comparison of neural inputs estimated with the model (upper traces), and the rectified EMG in mV (lower traces), for anteflexion (left) and retroflexion (right): (a) deltoideus, pars anterior (delcl), media (dels6) and posterior (dels2); (b) latissimus dorsi; (c) pectoralis major, pars clavicularis (pcc13 and EMG) and thoracalis (pcth2 and pcth4); (d) serratus anterior; (e) trapezius pars transversalis (within pars scapularis); (f) infraspinatus; (g) biceps brachii, biclo = caput longum, bicbr = caput breve, biceps = EMG representing both caput longum and breve.

shows a good correspondence between lati3 and the EMG. The small EMG burst around $t = 0.05$ s during anteflexion is not reproduced by the model but such activity was not found either in most other subjects.

Pectoralis major: Figure 4c shows the predicted inputs for three representative elements of the pectoralis major. Apparently, in the simulation, the pars clavicularis hardly shows agonist activity during anteflexion where the EMG does show such activity. Results from other subjects indicate a similar activity in the pars clavicularis and thoracalis of the pectoralis major which corresponds well to the average of the neural inputs in Fig. 4c.

Serratus anterior: Figure 4d demonstrates a good correspondence of the predicted inputs with the EMG of the serratus anterior. Both contain a clear triphasic pattern with agonist activity during anteflexion and antagonist activity during retroflexion. In Happee (1992b), in the thoracoscapular muscles, antagonist patterns were rarely found. However, in later measurements (Happee, 1993b; and unpublished results) in most subjects antagonist activity was found in the serratus anterior during retroflexion.

Trapezius: Figure 4e shows the predicted input of a part of the trapezius which should match the EMG of the trapezius pars transversalis. These are in reasonable agreement during anteflexion. During retroflexion the first EMG burst is well predicted by the model but the second is not. As a whole, the predictions for the trapezius are hard to validate as large differences between subjects were observed in the EMG of the three parts recorded (trapezius pars descendens, transversalis and ascendens).

Infraspinatus: Figure 4f shows that during both anteflexion and retroflexion activity of the infraspinatus is predicted near the movement onset. Such activity is also found in the EMG in Fig. 4f and in

other subjects. Thus the model supports the experimental finding that the infraspinatus cannot be simply classified as an anteflexor or a retroflexor. The predicted activity around $t = 0.2$ during retroflexion is not well matched by the EMG in Fig. 4f and in other subjects.

Biceps brachii: Figure 4g shows the predicted activity in the biceps brachii which corresponds well with the EMG only during anteflexion. This indicates a limited value of the simulation results for the biceps. The predictions in the biceps brachii and triceps brachii also are of a limited value since the elbow is incompletely described in the current model.

Overview of stresses and forces

Figure 5 shows all muscle stresses. Most stresses are relatively low compared to the maximal isometric stress of $100\,\mathrm{N\,cm^{-2}}$. This is partially due to the force–velocity relation which causes a reduction of the maximal stress to about $40\,\mathrm{N\,cm^{-2}}$ in several muscle parts. Furthermore, the predicted muscle inputs are largely submaximal as is illustrated in Fig. 4. The largest stress is predicted in the biceps brachii caput longum which is the only muscle in which maximal inputs are estimated (Fig. 4g).

Reaction forces and constraints: Figure 6 shows the reaction forces at the scapulothoracic gliding plane, in the conoid ligament and in the glenohumeral joint. As can be seen in Fig. 6, the contact force at the angulus inferior (AI) is positive throughout both the anteflexion and the retroflexion movement. This indicates that the inequality constraint that this force must be at least zero is not active; the constraint does not affect the solution. The reaction force at the trigonum spinae (TS) is positive in the first phase of the anteflexion movement and in a later phase of the retroflexion movement. The inequality constraint is active for the rest of the time. Thus in the antagonist phase of the anteflexion movement and the agonist phase of the retroflexion movement, muscle forces have to be adapted to let the force at the TS be at least zero and thus to maintain contact between the thorax and the scapula. In these phases, retroflexor activity is required for either deceleration or acceleration. To assess the muscular contributions to the TS force, the model was also simulated without the TS constraint. Comparing the results with the normal simulations, it was found that considerably increased activity was required to satisfy the TS constraint, mainly in the trapezius pars scapularis and in the levator scapulae. Furthermore, without the TS constraint, the pectoralis minor remained completely inactive. The TS constraint had negligible effects on the estimated activity of the first 5 (lower) parts of the serratus anterior, which show anteflexor activity as illustrated in Fig. 4d. The upper part (part 6) showed agonist activity during retroflexion. This activity was found only when the TS constraint was active, and thus apparently contributes to the TS force. Such a contribution of the upper part (parts 5,6) of the serratus anterior to the TS stability constraint was also found during static abduction (Van der Helm, 1994b).

The tension force in the conoid ligament was positive throughout both the anteflexion and the retroflexion movement. Only in the rest position (15° retroflexion) before anteflexion was a zero conoid force found.

Glenohumeral constraint: The trace *GH* in Fig. 6 describes the glenohumeral reaction force. Large contact forces are estimated throughout both the anteflexion and the retroflexion movement. The traces *theta* and *phi* in Fig. 6 describe the direction of the glenohumeral reaction force. This direction is described more clearly in Fig. 7 which also illustrates the stability of the glenohumeral joint. This stability was included as a nonlinear inequality constraint in the model. Figure 7 shows the behavior of the glenohumeral constraint during anteflexion. The reaction force is first directed close to the ellipse describing the rim of the glenoid cavity and then moves to a more central position. During retroflexion the force describes a similar path in the opposite direction. The constraint requires that the joint reaction force stays within the ellipse. As illustrated in Fig. 7 the ellipse is never met and thus the constraint is not active; it does not affect the solution. In preliminary simulations with different model parameters the constraint became active during several phases of the movements. Omitting the constraint yielded a glenohumeral force in a direction almost tangential to the glenoid joint surface. These potentially dangerous conditions occurred at times when the overall force levels were very low. In these conditions only slight modifications of muscle forces were required to satisfy the glenohumeral constraint. When this also holds for other conditions it will be very difficult to detect such modifications experimentally from the EMG. Thus it will be practically impossible to discriminate between the muscular coordination of the patient with habitual luxation and the normal coordination.

Energy and scapular motion

The mechanical energy delivered and dissipated by muscles is presented in Table 3. Until now (Figs 3–7) a scapular movement according to the scapulohumeral rhythm was assumed. Table 3 also describes results of simulations performed with a fixed scapula; its position was kept constant but the movement equations specifying equilibrium of the scapula were still to be satisfied. The scapular motion strongly affects the mechanical energy delivered by muscles (Table 3). Energy is mainly delivered to accelerate the limb and dissipated to decelerate the limb. This was verified from plots of the mechanical power delivered by individual muscle elements as a function of time, where it emerged that during acceleration very little power is dissipated. In the simulation with scapular motion, the thoracoscapular muscles deliver a considerable amount of energy. Of course, with a fixed

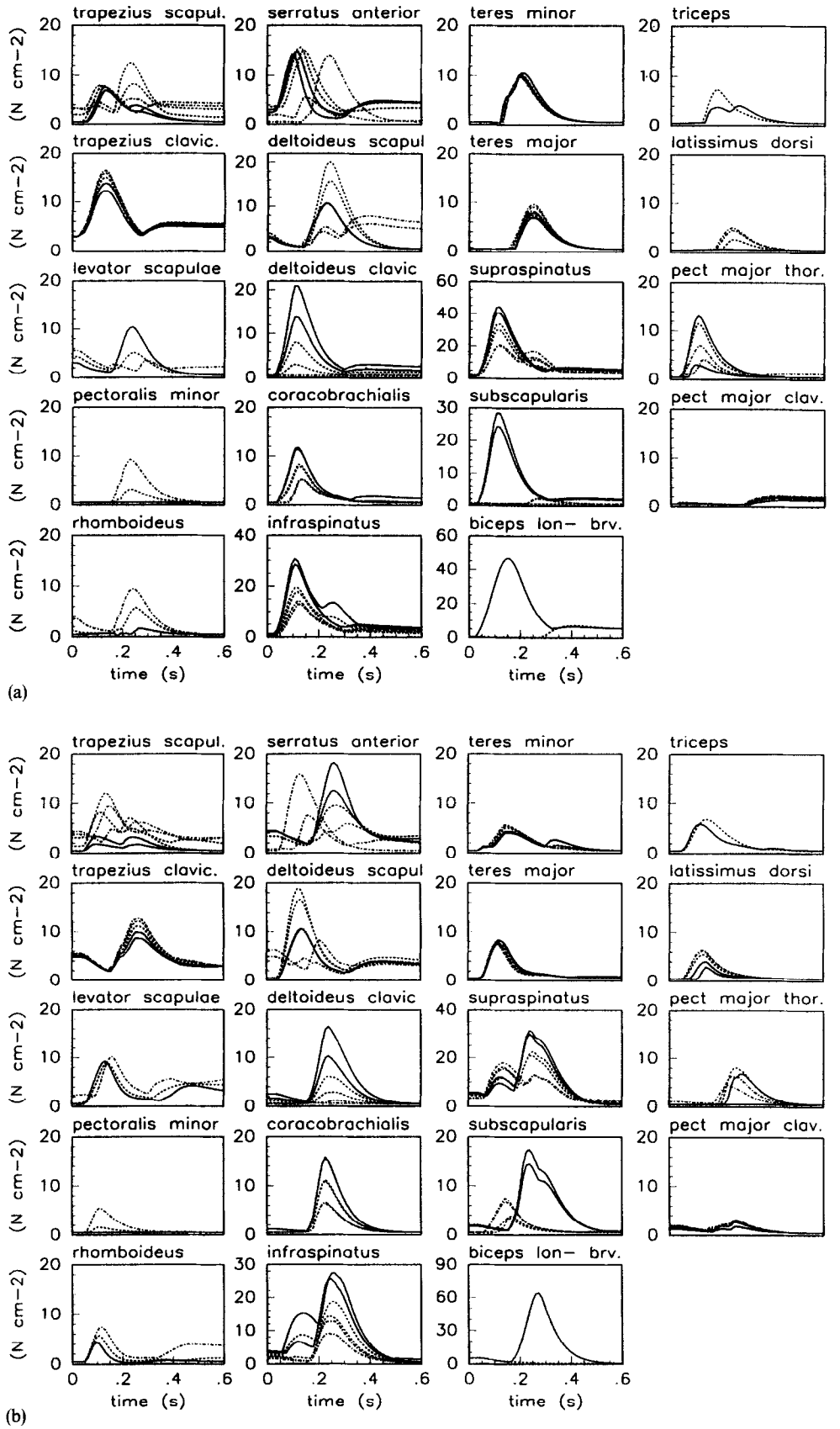

Fig. 5. Muscle stresses predicted, (a) anteflexion, (b) retroflexion: (——) first element(s); (– – –) middle element(s); (–·–·–) last element(s).

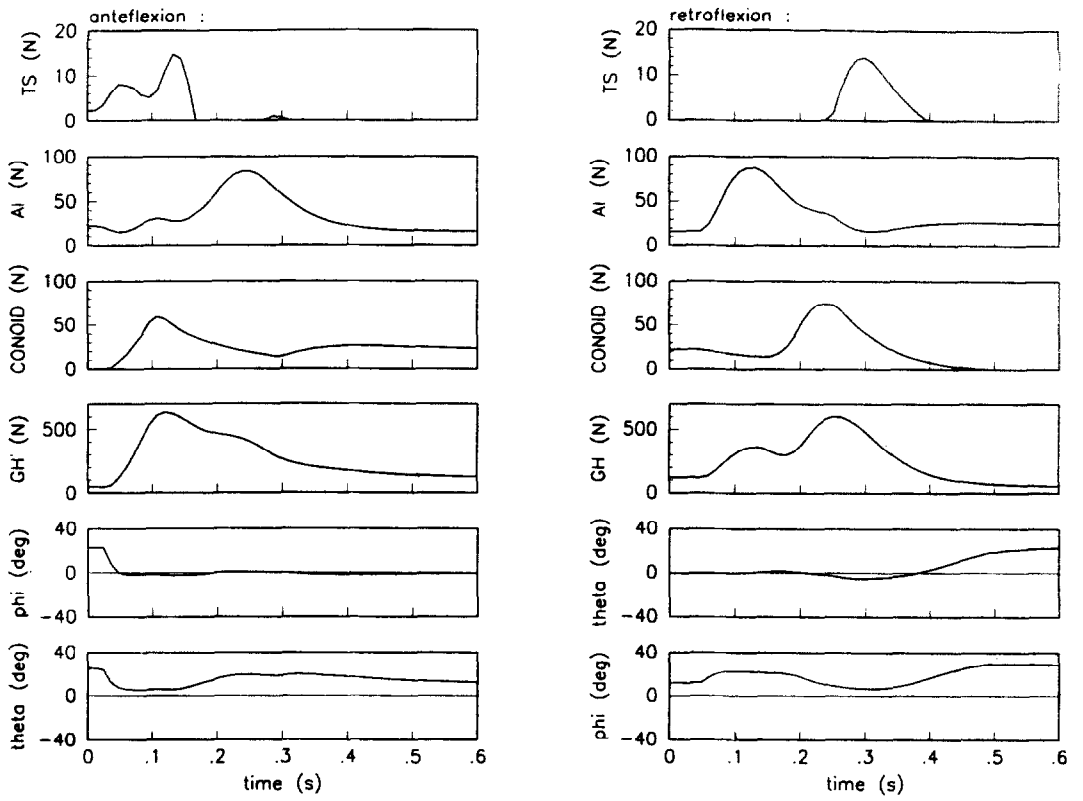

Fig. 6. Reaction forces, (TS) trigonum spinae; (AI) angulus inferior; (conoid) conoid ligament tension force; (GH) glenohumeral resultant force; theta and phi describe the direction of the glenohumeral force as illustrated in Fig. 7.

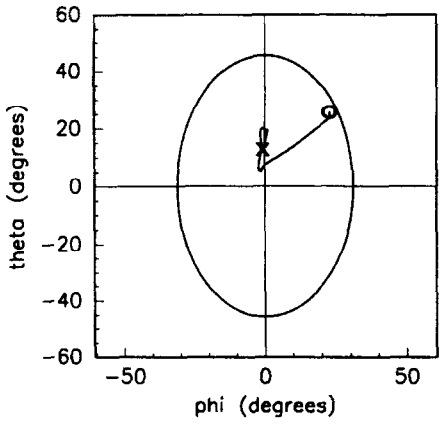

Fig. 7. The glenohumeral constraint during anteflexion. The curve describes the intersection of the joint reaction force vector with the articular surface of the glenoid. The ellipse describes the border of the glenoid cavity, as viewed from a lateral position. Axes are in degrees, (right) anterior, (up) cranial. (0) the initial position, (x) the final position.

scapula the thoracoscapular muscles cannot deliver any energy as their length is constant. With a fixed scapula, the muscles with an origin on the scapula and insertion on the humerus have an increased length change and therefore deliver more energy. These effects of scapular motion have also been evaluated with respect to the shortening velocities. With scapular movement, the lower element of the rhomboideus attained about 65% of its maximal shortening velocity which is much more than the 20–30% at which muscular energy generation is most efficient. The shortening velocity of most other muscles was about 25%. The scapular motions affect the metabolic cost required to obtain the desired forces. This cost is represented by the criterion optimized [Equation (1)]. The summed criterion over the whole anteflexion movement is increased 13% when no scapular movement is allowed. Similarly during retroflexion the criterion is increased 6%. This indicates that the assumed scapular movement reduces the metabolic cost.

Besides the shortening velocities the movements of the scapula also affect the muscular moment arms and the stability of the glenohumeral joint. From separate simulations it emerged that the moment arms affect the summed cost by less than 0.7%. The glenohumeral stability is positively affected by the scapular motion: In the retroflexed position, marked **0** in Fig. 7, with scapular motion no force modifications are required to obtain a stable glenohumeral joint. Without scapular motion the force moves to the ellipse and minor force modifications are required to stabilize the joint.

Table 3. Mechanical energy in Nm, delivered and dissipated during anteflexion (left) and retroflexion (right), the value in brackets ( ) is computed without scapular motion, the energy is computed as the product of force and shortening velocity integrated over the whole movement

	Anteflexion		Retroflexion	
Muscle (part)	Delivered	Dissipated	Delivered	Dissipated
Trapezius pars scapularis	0.35 (0)	0.16 (0)	0.18 (0)	0.20 (0)
Trapezius pars clavicularis	0.15 (0)			0.13 (0)
Levator scapulae		0.24 (0)	0.30 (0)	
Pectoralis minor		0.01 (0)	0.01 (0)	
Rhomboideus		0.57 (0)	0.36 (0)	
Serratus anterior	1.09 (0)		0.03 (0)	1.45 (0)
Subtotal scapular muscles	1.59 (0)	0.98 (0)	0.88 (0)	1.78 (0)
Infraspinatus	0.47 (0.74)	0.02 (0.06)	0.03 (0.06)	0.50 (0.78)
Supraspinatus	0.21 (0.56)	0.03 (0.03)	0.04 (0.04)	0.17 (0.53)
Subscapularis	0.08 (0.18)	0.08 (0.08)	0.22 (0.24)	0.05 (0.11)
Teres minor		0.06 (0.09)	0.04 (0.13)	
Subtotal rotator cuff muscles	0.76 (1.48)	0.19 (0.26)	0.33 (0.47)	0.62 (1.42)
Deltoideus pars scapularis	0.03 (0.08)	1.15 (1.26)	1.12 (1.32)	0.08 (0.15)
Deltoideus pars clavicularis	0.18 (0.50)			0.16 (0.38)
Coracobrachialis	0.15 (0.09)			0.22 (0.14)
Teres major		1.06 (1.95)	0.89 (1.05)	
Biceps brachii caput longum	0.81 (1.24)			0.72 (1.15)
Biceps brachii caput breve	0.02 (0.02)			0.04 (0.06)
Triceps brachii caput longum		0.20 (0.21)	0.24 (0.36)	
Latissimus dorsi		0.30 (0.17)	0.54 (0.60)	
Pectoralis major pars thoracalis	0.40 (0.40)			0.31 (0.39)
Pectoralis major pars clavicularis	0.01 (0.02)			0.02 (0.08)
Total of all muscles	3.95 (3.83)	3.88 (3.85)	4.00 (3.80)	4.05 (3.77)

DISCUSSION

Fast goal directed arm movements in the sagittal plane were analyzed with a three-dimensional shoulder model. The simulations provided estimates of the activity of shoulder muscles including the activity of deeper lying muscles. Table 3 for instance shows the large amount of energy contributed by the teres major to retroflexion.

The model

Three-dimensional models of shoulder kinematics have been presented by Engin and Peindl (1987), by Pronk (1989, 1991) and by Högfors *et al.* (1991). Muscle forces have been included by Högfors *et al.* (1987) and by Karlsson and Peterson (1992). A three-dimensional dynamic shoulder model, including inertia and muscle forces was recently developed (Van der Helm, 1994a, b; Van der Helm and Veenbaas, 1991; Van der Helm *et al.*, 1992; Veeger *et al.*, 1991). In the current paper, muscular dynamics have been included into this shoulder model. This is done with the method of inverse dynamic optimization including muscular dynamics developed by Happee (1994).

The activity estimated with the model has been compared with surface EMG measurements (Fig. 4). EMG measurements are informative with respect to timing rather than amplitude of muscular activity. Most model results were similar to the EMG but some differences between model results and EMG were found in muscles where the EMG activity was subject dependent.

As described in the section *Kinematic and EMG data*, the assumed movements of the scapula and the clavicle were based on static measurements performed on other subjects. For dynamic measurement of these movements, the possibility of three-dimensional roentgen is currently assessed in our group. The consequence of the assumed scapular movement has been evaluated by performing an additional simulation without scapular movement. A marked effect was found on the muscular shortening velocities and on the mechanical energy contributions (Table 3). Furthermore, in the simulation without scapular movement the summed metabolic cost criterion [Equation (1)] was increased 13% for the anteflexion movement and 6% for the retroflexion movement. This indicates that the scapular movement assumed in the normal simulation reduces the metabolic cost.

Muscle elements: Because many shoulder muscles have a complex three-dimensional geometry, muscle fibers have different lines of action and therefore have different mechanical effects. Van der Helm and Veenbaas (1991) analyzed the mechanical effect of shoulder muscles and showed that, depending on the muscle geometry, at most 6 elements per muscle are required

to obtain a sufficiently accurate description of the mechanical effect of muscles (Table 1). Figures 4 and 5 show large differences between the predicted activity in different elements of the same muscle. As these forces are predicted by optimization of a mechanical criterion, this shows the mechanical relevance of modelling so many muscle elements. Another point is to what extent the nervous system can selectively activate muscle elements. The motor-neuron pool and the motor-unit distribution in muscles may constrain this selectivity. In the solution of the load sharing problem it may be relevant to include neural constraints on the differences between activations of muscle elements. On the other hand, the current results contain a rather gradual change of the activation through muscles: No extreme differences were predicted between the activity of adjacent muscle elements.

Muscular dynamics: The inclusion of muscular dynamics into the model had a considerable effect on the neural inputs and forces predicted (Fig. 3). In the EMG a large difference in timing was observed between two synergist muscles, the latissimus dorsi and the deltoideus pars posterior. Activity of the latissimus dorsi preceded the deltoideus pars posterior by up to 62 ms (Table 3 in Happee, 1992b). In Happee (1992b) it was suggested that this phenomenon can be explained by the fact that the latissimus has longer muscle fibers and a longer tendon than the deltoideus pars posterior and therefore (probably) exhibits a slower response of force to activation. The earlier activation of the latissimus was suggested to be a compensation, generated in the nervous system, for the slower response of the latissimus. In the model results no relevant difference in timing has been found. This can be explained by the fact that all muscles are modelled as having equal active state dynamics and neural activation dynamics (Table 2). The mechanical dynamics are determined by the ratio of the maximum shortening velocity and the series elastic stretch. As both these parameters were taken proportional to muscle length, in the current model, muscle length does not affect muscular dynamics, which seems a point of interest in further modelling.

Thoracoscapular muscles

The mechanical energy contributions in Table 3 show that thoracoscapular muscles contribute strongly to the acceleration and deceleration of the limb. The serratus anterior delivers 28% of the positive energy during anteflexion and dissipates 35% of the energy during retroflexion. The rhomboideus delivers 9% of the positive energy during retroflexion and dissipates 15% of the energy during anteflexion.

Furthermore, considerable activity of thoracoscapular muscles is shown to be required to satisfy the TS constraint. This constraint represents that the trigonum spinae of the scapula has to stay in contact with the thorax. This constraint was also shown to be active during abduction (Van der Helm, 1991). Contact between the thorax and the scapula is very relevant, as this contact makes the shoulder a closed-chain mechanism (thorax-clavicle-scapula-thorax). Due to this closed-chain the clavicle and the scapula provide a mechanically stable base for the glenohumeral joint.

In Happee (1992b) in the EMG of thoracoscapular muscles antagonist activity was rare. This left unclear how decelerating forces induced by the prime movers are transferred to the trunk. Meanwhile, measurements in other subjects showed antagonist activity in the serratus anterior during retroflexion as is also predicted by the model (Fig. 4d). During anteflexion in thoracoscapular muscles no clear antagonist patterns were simulated. Yet the decelerating forces can be transferred to the trunk by the more complicated activity of, for instance the trapezius pars scapularis, where this activity is also related to the TS constraint.

Stability of the glenohumeral joint

Van der Helm (1994b) showed that modifications of muscle forces are required to stabilize the glenohumeral joint during posture maintenance. He found increased forces in the so-called rotator cuff muscles, four muscles inserting as a half circle close to the glenohumeral joint. These results support the conclusion that rotator cuff muscles actively stabilize the glenohumeral joint. The current paper presents the first evaluation of glenohumeral stability in dynamic conditions. In the goal directed movements analyzed, considerable muscle forces are required to accelerate and decelerate the limb. However, it was found that the glenohumeral constraint is not active during acceleration and deceleration; the constraint does not affect the solution. Apparently, the force distribution resulting from the optimization of the criterion [Equation (1)] provides a stable joint. Thus the current results provide no indication that voluntary accelerations are critical with respect to humerus dislocation. This observation is, however, based on simulations in a small movement range and certainly cannot be extended to extreme movements like baseball pitching.

A relatively large stress was found in 3 of the 4 rotator cuff muscles: the infraspinatus, supraspinatus and subscapularis (Fig. 5). This large stress is a result of the cost criterion optimized [Equation (1)] containing a weighting of muscle volume (motivated in Happee and van der Helm, 1994). The volume is proportional to muscle fiber length, thus a larger cost will be attributed to stress in longer muscles. Minimization of the cost criterion will therefore attribute a relatively large stress to shorter muscles like those of the rotator cuff. This accounts for agonist activity in rotator cuff muscles. Here agonist activity is defined as contributing somehow to the net torques required at a certain instant. It has been suggested that even antagonistic cuff activity should be required to stabilize the joint (Van der Helm, 1994a). Antagonist activity will never be predicted by any criterion of a form like equation (1). Antagonist activity can be enforced by the

glenohumeral constraint but this was not the case in the current simulations as the constraint was not active; the constraint did not affect the solution. According to Table 3 rotator cuff muscles deliver considerable positive energy: The infraspinatus and supraspinatus contribute to anteflexion and the subscapularis to retroflexion. This once more indicates agonist activity of rotator cuff muscles.

REFERENCES

Basset, R. W., Browne, A. O., Morrey, B. F. and An, K. N. (1990) Glenohumeral muscle force and moment dynamics in a position of shoulder instability. *J. Biomechanics* **23,** 405–415

Crowninshield, R. D. and Brand, R. A. (1981) A physiologically based criterion of muscle force prediction in locomotion. *J. Biomechanics* **14,** 793–801.

Dul, J., Townsend, M. A., Shiavi, R. and Johnson, G. E. (1984a) Muscular synergism—I: On criteria for load sharing between synergistic muscles. *J. Biomechanics* **17,** 663–673.

Dul, J., Johnson, G. E., Shiavi, R. and Townsend, M. A. (1984b) Muscular synergism—II. A minimum-fatigue criterion for load sharing between synergistic muscles. *J. Biomechanics* **17.** 675–684.

Engin, A. E. (1980) On the biomechanics of the shoulder complex. *J. Biomechanics* 13-7; 575–590.

Engin, A. E. and Peindl, R. D. (1987). On the biomechanics of human shoulder complex—I. Kinematics for determination of the shoulder complex sinus. *J. Biomechanics* **20,** 103–117.

Flanders, M. and Soechting, J. F. (1990) Arm muscle activation for static forces in three dimensional space. *J. Neurophysiology* **64,** 1818–1837.

Happee, R. (1992a) Time optimality in the control of human movements. *Biological Cybernet.* **66,** 357–366.

Happee, R. (1992b) Goal-directed arm movements. I. Analysis of EMG records in shoulder and elbow muscles. *J. Electromyogr. Kinesiol.* **2,** 165–178.

Happee, R. (1993a) Goal-directed arm movements. II: A kinematic model and its relation to EMG. *J. Electromyogr. Kinesiol.* **3,** 13–23.

Happee, R. (1993b) Goal-directed arm movements. III: Feedback and adaptation in response to inertia perturbations. *J. Electromyogr. Kinesiol.* **3,** 112–122.

Happee, R. (1994) Inverse dynamic optimization including muscular dynamics, a new simulation method applied to goal directed movements. *J. Biomechanics* **27,** 953–960.

Happee, R. and Van der Helm, F. C. T. (1994) Criteria representing the cost of muscular contraction, used to solve the load sharing problem in inverse dynamic optimizations (submitted).

Hatze, H. (1981) Myocybernetic control models of skeletal muscle, characteristics and applications. University of South Africa, ISBN 0 86981 216 5.

Högfors, C., Sigholm, G. and Herberts, P. (1987) Biomechanical model of the human shoulder—I: Elements. *J. Biomechanics* **20,** 157–166.

Högfors, C., Peterson, B., Sigholm, G and Herberts, P. (1991) Biomechanical model of the human shoulder joint—II: The shoulder rhythm. *J. Biomechanics* **24,** 699–709.

Inman, V. T., Saunders, J. B. and Abbot, L. C. (1944) Observations on the function of the shoulder joint. *J. bone Jt surg.* **26a,** 1–30.

Karlsson, D. (1992) Force distributions in the human shoulder. Ph.D. Thesis, Göteborg.

Karlsson, D. and Peterson, B. (1992) Towards a model for force predictions in the human shoulder. *J. Biomechanics* **25,** 189–199.

Lippitt, S. and Mattsen, F. (1993) Mechanism of glenohumeral joint stability. *Clini. Orthop. Related Res.* **291,** 20–28.

Patriarco, A. G., Mann, R. W., Simon, S. R. and Mansour, J. M. (1981) An evaluation of the approaches of optimization models in the prediction of muscles forces during human gait. *J. Biomechanics* **14,** 513–525.

Pedersen, D. R., Brand, R. A., Cheng, C. and Aurora, J. S. (1987) Direct comparison of muscle force predictions using linear and nonlinear programming. *J. biomech. Engng* **109,** 192–198.

Pedotti, A., Krishan, V. V. and Stark, L. (1978) Optimization of muscle-force sequencing in human locomotion. *Math. Biosci.* **38,** 57–76.

Pronk, G. M. (1989) A kinematic model of the shoulder girdle: a resume. *J. Med. Eng. Technol.* **13,** 119–123.

Pronk, G. M. (1991) The shoulder girdle: analysed and modelled kinematically. Ph.D. Thesis, Delft University of Technology, The Netherlands, ISBN 90-370-0053-3.

Pronk, G. M. and Van der Helm, F. C. T. (1991) The palpator, an instrument developed for measuring the 3-D positions of bony landmarks in a fast and easy way. *J. Med. Engng Technol.* **15,** 15–20.

Ruitenbeek, J. C. and Jansen, R. J. (1984) Computer controlled manipulator display system for human movement studies. *Med. Biological Engng Comput.* **22,** 304–308.

Van der Helm, F. C. T. (1994a) A finite element musculoskeletal model of the shoulder mechanism. *J. Biomechanics* **27,** 551–569.

Van der Helm, F. C. T. (1994b) Analysis of the kinematic and dynamic behavior of the shoulder mechanism. *J. Biomechanics* **27,** 527–550.

Van der Helm, F. C. T. and Veenbaas, R. (1991) Modelling the mechanical effect of muscles with large attachment sites: application to the shoulder mechanism. *J. Biomechanics* **24,** 1151–1163.

Van der Helm, F. C. T. and Pronk, G. M. (1994) Three-dimensional recording and description of the motions of the shoulder mechanism. *J. biomech. Engng.* (accepted).

Van der Helm, F. C. T., Veeger, H. E. J., Pronk, G. M., Van der, Woude L.H.V. and Rozendal, R.H. (1992) Geometry parameters for musculoskeletal modelling of the shoulder mechanism. *J. Biomechanics* **25,** 129–144.

Veeger, H. E. J., Van der Helm, F. C. T., Van Der Woude, L. H. V., Pronk, G. M. and Rozendal, R. H. (1991) Inertia and muscle contraction parameters for musculoskeletal modelling of the shoulder mechanism. *J. Biomechanics* **24,** 615–629.

Winters, J. M. and Stark, L. (1985) Analysis of fundamental human movement patterns through the use of in-depth antagonistic muscle models. *IEEE Trans Biomed Engng.* **BME-32-10,** 826–839.

Winters, J. M. and Stark, L. (1988) Estimated properties of synergistic muscles involved in movements of a variety of human joints. *J. Biomechanics* **21,** 1027–1041.